crystals

MDPI

Article

The Crystal Structure of Mg–Al–CO_3 Layered Double Hydroxide

Elena S. Zhitova [1,*], Rezeda M. Sheveleva [1,2], Andrey A. Zolotarev [1,2] and Sergey V. Krivovichev [2,3]

[1] Institute of Volcanology and Seismology, Far East Branch of Russian Academy of Sciences, Petropavlovsk-Kamchatsky 683006, Russia; st034435@student.spbu.ru (R.M.S.); andrei.zolotarev@spbu.ru (A.A.Z.)
[2] Saint-Petersburg State University, Saint-Petersburg 199034, Russia; s.krivovichev@ksc.ru
[3] Kola Science Centre, Apatity 189209, Russia
* Correspondence: zhitova_es@mail.ru

Abstract: The crystal structure of quintinite, $Mg_4Al_2(OH)_{12}(CO_3)\cdot 3H_2O$, from the Jacupiranga alkaline complex (Cajati, São Paulo, Brazil), was refined for two samples (91002 and C7029) using single-crystal X-ray diffraction data. The mineral crystallizes in the *P*-3*c*1 space group, a = 5.246/5.298, c = 15.110/15.199 Å for samples 91002/C7029. The crystal structure consists of octahedral sheets with Mg and Al ordering according to a $\sqrt{3} \times \sqrt{3}$ superstructure. The Mg and Al atoms are coordinated by six hydroxylated oxygen atoms; the average <Mg–O> and <Al–O> bond distances are in the ranges 2.022–2.053 Å and 1.974–1.978 Å, respectively. The interlayer structures are identical (in contradiction to the previous assumptions), and consist of disordered $(CO_3)^{2-}$ groups and $(H_2O)^0$ molecules. The samples from Jacupiranga can be identified as quintinite-2*T*, which is the second finding of this polytype after the Kovdor alkaline complex (Kola peninsula, Russia). The powder X-ray diffraction pattern of quintinite-2*T* contains weak superstructure reflection at 4.57 Å (010), indicative of Mg and Al ordering. An important crystal-chemical criterion of quintinite is the interlayer distance (d_{00n}-value) of ~7.56 Å, which is steady among natural specimens from various findings worldwide.

Keywords: quintinite; hydrotalcite; layered double hydroxide; natural; mineral; crystal structure; carbonate; cation ordering; Jacupiranga

Citation: Zhitova, E.S.; Sheveleva, R.M.; Zolotarev, A.A.; Krivovichev, S.V. The Crystal Structure of Mg–Al–CO_3 Layered Double Hydroxide. *Crystals* **2023**, *13*, 839. https://doi.org/10.3390/cryst13050839

Academic Editor: Zhaohui Li

Received: 3 May 2023
Revised: 16 May 2023
Accepted: 16 May 2023
Published: 19 May 2023

1. Introduction

Hydrotalcite supergroup minerals [1] are natural representatives of industrially applied Layered Double Hydroxides (LDHs) [2]. LDHs form a class of inorganic lamellar compounds with crystal structures consisting of alternating positively charged metal-hydroxide layers (octahedral sheets) and negatively charged interlayers [3,4]. LDHs can be represented by the general formula [5–7] $[M^{2+}{}_{1-x}M^{3+}{}_x(OH)_2][A^{n-}]_{x/n}\cdot mH_2O$, where M^{2+} = Mg^{2+}, Ni^{2+}, Fe^{2+}, Mn^{2+}, etc., and M^{3+} may be, e.g., Al^{3+}, Fe^{3+}, Cr^{3+} and other trivalent cations; x = 0.33 and 0.25 are the most common values and correspond to M^{2+}:M^{3+} = 2:1 and 3:1 ratios, respectively, which are the most widespread among LDHs; A^{n-} is the anion of the n negative charge (the most common among mineral are $CO_3{}^{2-}$, Cl^-, $SO_4{}^{2-}$, $Sb(OH)_6{}^-$); m is the number of interlayer H_2O molecules. This general formula is further extended by (i) minerals of the wermlandite group [8–11] and their synthetic counterparts [12–14] that contain additional interlayer mono- or divalent cations (like Na, K, Ca etc.), and by (ii) Li–Al (i.e., M^+–M^{3+}) LDHs, the structures of which are represented by gibbsite-like layers [15,16], with the general formula of such compounds given as $[Al_4Li_2(OH)_2][A^{n-}]_{x/n}\cdot mH_2O$.

Magnesium–aluminum LDHs with carbonate interlayers are among the longest known in the LDH family; they are applied as catalytic materials [17,18] and considered efficient and inexpensive oxygen evolution reaction electrocatalysts [19]. Mg–Al LDHs are often used as model systems for LDH families of different (rare) chemical compositions (for example, the substitution of cations while maintaining stoichiometry). Mg–Al–CO_3 LDHs

are applied in pharmacology as a Talcid medicine. Recent pharmaceutical studies involving Mg–Al LDHs include hybrid materials with glibenclamide [20], nanocarrier materials for antimicrobial chemotherapy [21], and a porous nanocomposite of LDH with chitosan for cosmetic application [22]. LDHs, including Mg–Al varieties, are considered sorbents of undesirable anions and cations; recent research includes methyl orange [23,24], Pb^{II} [25], Cu^{II} [26], and Congo red dye [27] removal from aqueous solutions, as well as harmful anion (such as Cl^-, Br^-, I^-, AsO_4^{3-}, etc.) sorption from fertile soil [28]. The uptake of Cl^- and CO_3^{2-} anions by Mg–Al and Ca–Al LDHs from pore solutions was simulated for cementitious materials [29]. The possibility of anion uptake by LDHs also makes them advanced materials for CO_2 capture [30]. The high industrial and material science interest towards LDHs requires a detailed understanding of the internal structure of these materials. Highly crystalline and extremely stable prototypes of such materials are natural compounds [31]—hydrotalcite supergroup minerals [1].

Despite the wide chemical variability of LDHs, their crystal structures show a certain structural commonality, in which one structural type extends to compounds of different compositions. For example, quintinite is isotypic to the Li–Al gibbsite-based mineral akopovaite, $Al_4Li_2(OH)_{12}CO_3 \cdot 3H_2O$ [32], following the substitution scheme $[Mg_4Al_2(OH)_{12}]^{2+} \rightarrow [Al_4Li_2(OH)_{12}]^{2+}$. Both structures show cation (Mg/Al or Al/Li) ordering according to $\sqrt{3} \times \sqrt{3}$ superstructures and identical schemes of interlayer species arrangement despite a rather principal chemical variability. The same applies to their Cl-analogues: chlormagaluminite, $Mg_4Al_2(OH)_2Cl_2 \cdot 3H_2O$, [33], and dritsite, $Al_4Li_2(OH)_{12}Cl_2 \cdot 3H_2O$ [34]. Comparison of the crystal structures of minerals shows that they are isotypic to their synthetic analogues, which is well shown by Li–Al LDHs [35–37]. Therefore, the crystal structures obtained for minerals through single-crystal X-ray diffraction analysis (the technique that makes it possible to obtain models of crystal structures with greater accuracy) can be extended to industrially applied synthetic LDH materials.

In this study, we provide crystal chemical characterization of quintinite from Jacupiranga (São Paulo, Brazil). Previously, the crystal structure of quintinite from that locality was described as stratified with two types of interlayers (see details below), which contradicts the more recent studies of quintinite from the Kovdor complex [38–42]. The goal of the present study is to resolve this contradiction, i.e., to check whether quintinites from different localities are isotypic to each other or not. In addition, we provide data that should be helpful for the identification of cation-ordered polytypes with hexagonal stacking sequences using a powder X-ray diffraction method.

Previous Crystal Structure Studies of Quintinite

The first crystal structure study of quintinite (at that time—"manasseite", i.e., hydrotalcite) was carried out on a sample from Jacupiranga [43]. The study demonstrated the presence of Mg and Al ordering according to a $\sqrt{3} \times \sqrt{3}$ superstructure in the metal-hydroxide layer (or octahedral sheet), hexagonal layer stacking sequence and stratified interlayer that consisted of two types: (i) (H_2O) molecules and (ii) $(CO_3)^{2-}$, which alternated along the *z* direction [43] (Figure 1).

Almost simultaneously, quintinite was approved as a separate (from hydrotalcite/manasseite) mineral species on samples from the alkaline complex of Mont Saint-Hilaire, Quebec, Canada [44]. The crystal structure was not refined, but unit-cell parameters determined were indicative of polytypes with hexagonal and rhombohedral layer stacking sequences doubled in comparison to previous data [43] with lattice parameter *a* according to a $2\sqrt{3} \times 2\sqrt{3}$ superstructure (which, however, has not been identified elsewhere else) (Figure 2).

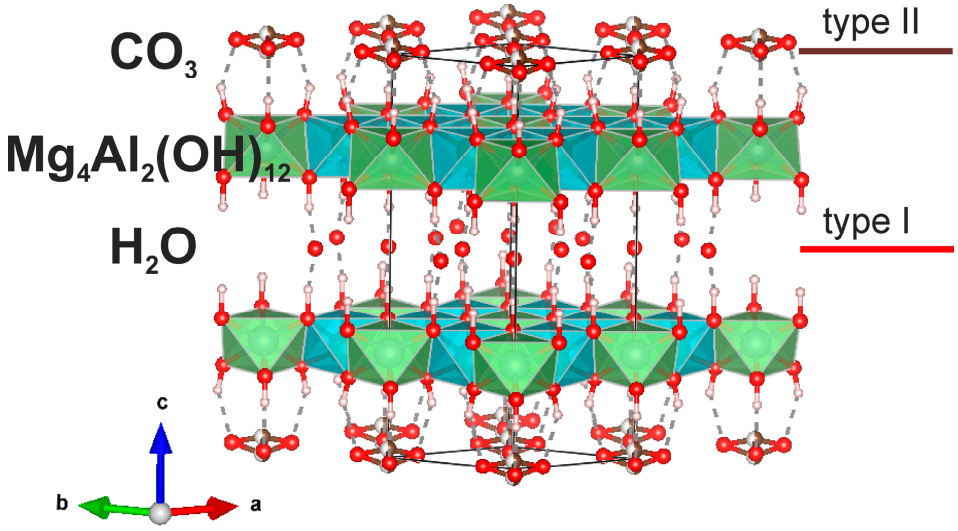

Figure 1. The crystal structure of quintinite from the Jacupiranga alkaline complex (Brazil) with stratified interlayers obtained previously (visualized using public cif-file) [43].

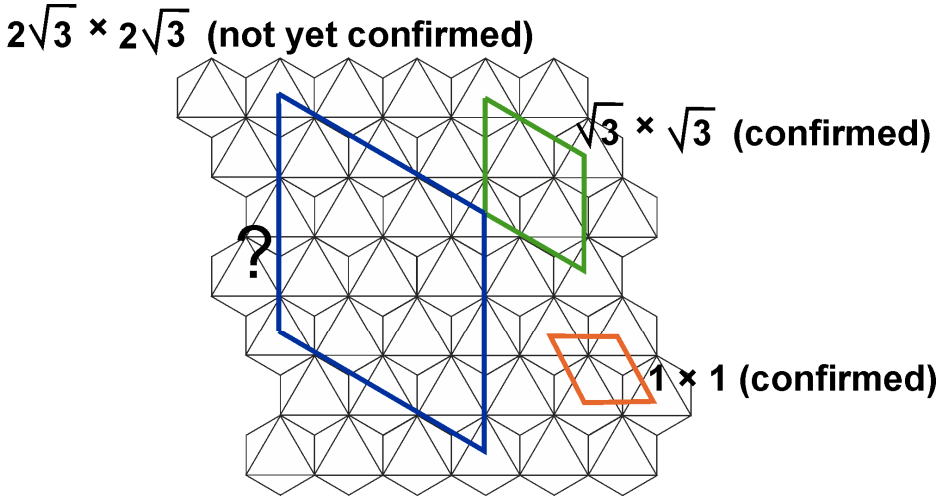

Figure 2. The superstructures within the octahedral sheet of LDHs, suggested for quintinite (see text for details). Different colours correspond to different in-plane structures: 1×1 (brown); $\sqrt{3} \times \sqrt{3}$ (green); $2\sqrt{3} \times 2\sqrt{3}$ (dark blue)—not yet confirmed.

We studied the polytypism of quintinite from the Kovdor alkaline complex (Kola peninsula, Russia), where the polytype character depends upon the following factors: (i) disorder or order of cations within a metal-hydroxide layer and (ii) type of layer stacking [38–42]. In total, five polytypes of quintinite were described in Kovdor; among them, 2*H*, 2*T*, 3*R* and 1*M* polytypes appear commonly (Figure 3). In addition, it was shown that the sequence of polytype formation can be described as $2H \rightarrow 2T \rightarrow 1M$. The polytype 2*T*-3*c* (or 2*H*-3*c* in the original version) can be characterized as a cell of 2*T* polytype shifted along the *z* direction, producing tripling of the number of layers within the unit cell; this polytype was observed in only one sample. Later, the study of "hydrotalcite" from two localities in the Ural Mountains (Russia), Ural emerald mines (Malyshevskoe or former Mariinskoe deposit) [45] and Bazhenovskoe chrysotile–asbestos deposit [46], demonstrated that Ural samples are in fact quintinite-1*M* (previously identified as hydrotalcite) isotypic to the Kovdor quintinite-1*M*. Recently, quintinite-1*M* was described from Mount Mather Creek, British Columbia, together with the 3*T*(?) polytype, which possesses some residual reflections [47].

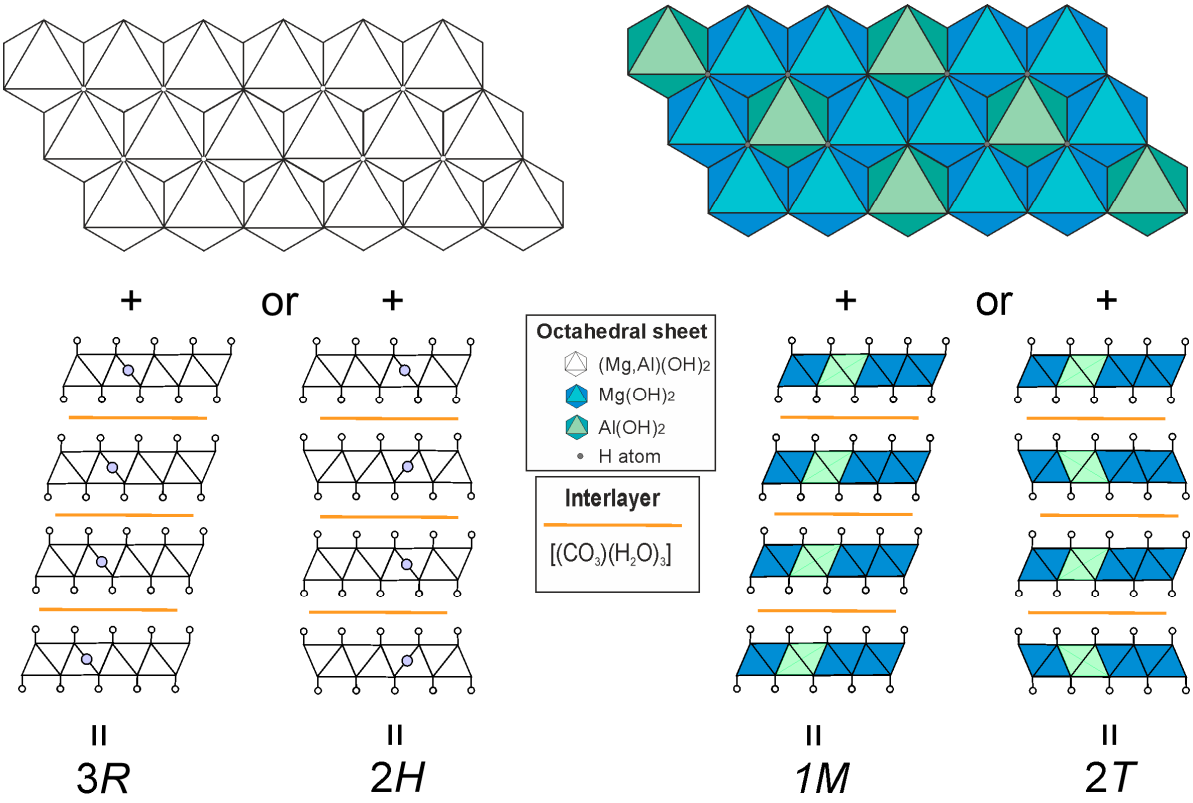

Figure 3. Schematic representation of quintinite, $Mg_4Al_2(OH)_{12}(CO_3) \times 3(H_2O)$, polytypes 3*R*, 2*H*, 1*M* and 2*T*.

2. Materials and Methods

2.1. Materials

Two samples from the Jacupiranga alkaline complex (Cajati, São Paulo, Brazil) labelled as "manasseite" were investigated from the following sources: (a) the systematic collection of the Fersman Mineralogical Museum of the Russian Academy of Science (Moscow, Russia) stored under catalogue number 91002 and (b) the collection of the Smithsonian Institution (National Museum of Natural History in Washington, DC, USA) stored under catalogue number C7029.

Originally, quintinite was described in Jacupiranga as "manasseite" (a hexagonal form of hydrotalcite that is currently discredited) [48]. Quintinite and manasseite/hydrotalcite have a confusing description history {see hydrotalcite's and quintinite's descriptions in Snarum (Norway) by [49–51]} because both are Mg–Al–CO_3 minerals with different Mg:Al ratios: 2:1 (quintinite) and 3:1 (hydrotalcite and formerly "manasseite"). The crystal structure of quintinite from the Jacupiranga mine was studied by [43], and the mineral was stated to be a potentially new mineral species from the "hydrotalcite-manasseite group" that had previously been described as "manasseite". Paying attention to the synchronism of this work on structure refinement (1996) [43] with the description of a new mineral—quintinite (1997) [44] and the subsequent citation of this structural work in the first description of quintinite, it is clear that the mineral from Jacupiranga studied by [43] was in fact quintinite. At the time of the description of its crystal structure, the name of quintinite had not yet been approved by the Commission on New Minerals, Nomenclature and Classification, and therefore is not mentioned in the text. The mineral is described as quintinite in the most recent study of the Jacupiranga minerals [52]. In Jacupiranga, quintinite was found in carbonatite rocks [48] and is considered a late-stage hydrothermal mineral.

2.2. Single-Crystal X-ray Diffraction

Single-crystal X-ray diffraction analysis was carried out for quintinite samples 91002 and C7029 using a Bruker Smart Apex diffractometer (X-ray diffraction Resource Center, St. Petersburg State University), Mo$K\alpha$ radiation, operated at 50 kV and 40 mA, equipped with a CCD area detector; more details on data collection are given in Table 1. The unit-cell parameters were refined using least-square methods. The data were processed using the *P*-3*c*1 space group. During data processing, we first successfully processed single-crystal X-ray diffraction data and refined the crystal structure in the $P6_3/mcm$ space group as the most probable option suggested by CrysAlisPro software package [53] (this space group was used for the refinement of chlormagaluminite structure [33]). However, this led to a large number of unaccounted-for reflections, as a result of which we decided to use the *P*-3*c*1 space group previously used for quintinite [42].

Table 1. Crystal data, data collection, and structure refinement details for quintinite samples 91002 and C7029.

Sample	91002	C7029
Crystal chemical data		
Crystal system	Trigonal	Trigonal
Space group	*P*-3*c*1	*P*-3*c*1
a (Å)	5.2459 (14)	5.2978 (5)
c (Å)	15.110 (5)	15.1991 (19)
V (Å^3)	360.1 (2)	369.44 (8)
Z	1	1
Calculated density (g/cm^3)	2.198	2.127
Absorption coefficient	0.486	0.472
Data collection		
Diffractometer	Bruker Smart APEX II	
Temperature (K)	293	
Radiation, wavelength (Å)	Mo$K\alpha$, 0.71073	
Range of data collection, 2θ (°)	5.392–67.174	5.36–72.626
h, *k*, *l* ranges	−7→6, −7→7, −21→21	−8→8, −8→8, −25→23
Total reflections collected	5549	6783
Unique reflections (R_{int})	406 (0.0324)	596 (0.0356)
Number of unique reflections $F > 2\sigma(F)$	320	424
Data completeness (%)	100	100
Structure refinement		
Refinement method	Full-matrix least-squares on F^2	
Weighting coefficients a, b	0.0410, 1.1022	0.0330, 1.5179
Data/restrain/parameters	406/2/34	596/2/34
R_1 [$F > 2\sigma(F)$], wR_2 [$F > 2\sigma(F)$]	0.0541, 0.1288	0.0678, 0.1384
R_1 all, wR_2 all	0.0685, 0.1378	0.0890, 0.1488
Goodness-of-fit on F^2	1.183	1.117
Largest diff. peak and hole (ēÅ^{-3})	0.38/−0.40	0.63/−0.56

The structure was solved and refined using the ShelX program package [54] incorporated into the Olex2 software shell [55], to R_1 = 0.053/0.066 for 320/424 independent reflections with $I \geq 2\sigma(I)$ for samples 91002 and C7029.

The positions of Mg, Al and oxygen in the metal-hydroxide layer were located by direct methods and refined anisotropically (Table S2). The interlayer species (O and C) and hydrogen atoms in the metal-hydroxide layer were located using the difference-Fourier maps and refined isotropically. The Mg, Al and O site occupancies (in the metal-hydroxide layer) were found to be close to 100% and fixed. Site occupancies of the interlayer atoms

were refined for O atoms and fixed for C atoms. The main crystallographic characteristics and structure refinement parameters are listed in Table 1.

2.3. Powder X-ray Diffraction

Powder X-ray diffraction (XRD) data were collected for sample 91002 using a Rigaku R-Axis Rapid II single-crystal diffractometer using Debye–Scherrer geometry (d = 127.4 mm). The diffractometer was equipped with a rotating anode (Co$K\alpha$, λ = 1.79026, voltage = 40 kV and current = 15 mA), microfocus optics and a cylindrical image plate detector. The data were converted using the Osc2xrd program [56].

The unit-cell parameters were refined via the Pawley method using Topas 4.2 [57], with the hexagonal structure model of space group *P*-3*c*1 and with the starting unit-cell parameters of sample 91002 reported herein. Refinement was based on the reflections in the 2θ region 10–60°. The indexing of the XRD pattern and refinement of the unit-cell parameters were performed with fixed atom coordinates, site scattering and isotropic displacement parameters. Neutral scattering factors were used for all atoms. The background was modelled using a Chebyshev polynomial approximation of the 14th order. The peak profile was described using the fundamental parameters approach. Refinement of preferred orientation parameters confirmed the presence of a significantly preferred orientation along the [001] direction.

3. Results

3.1. Crystal Structure Solution and Refinement

The collected single-crystal X-ray diffraction data were processed in the *P*-3*c*1 space group, a = 5.246/5.298 Å, c = 15.110/15.199 Å for samples 91002/C7029. Eight atomic positions were located from the structure solution and refinement for each quintinite sample (sites labelled): Mg, Al, O1 and H1 are part of the metal-hydroxide layer (or octahedral sheet) and fully occupied (Table 2).

Table 2. Atom coordinates, equivalent isotropic displacement parameters (Å^2), site occupancies and assigned site populations for quintinite samples 91002 and C7029.

Atom	x	y	Z	U_{eq}	s.o.f.	W.P.	Assigned Site Populations
Sample 91002							
Octahedral sheet							
Mg	0.3333	0.6667	0.4995 (1)	0.0069 (4)	0.3333 *	4d	
Al	0	0	0.5	0.0107 (5)	0.1667 *	2b	$Mg_4Al_2(OH)_{12}$
O1	0.3257 (5)	0.3262 (5)	0.5652 (1)	0.0145 (4)	1 *	12g	
H1	0.341 (9)	0.315 (9)	0.619 (3)	0.036 (12)	1 *	12g	
Interlayer gallery							
C1	0.3333	0.6667	0.745 (3)	0.010 (7)	0.033 *	4d	$(CO_3)_{1.0}(H_2O)_{3.0}$ **
C2	0.360 (4)	0	0.7500	0.028 (9)	0.05 *	6f	
O2	0.290 (3)	0.209 (2)	0.7514 (8)	0.033 (3)	0.280 (11)	12g	
O3	0.362 (3)	0.440 (2)	0.751 (1)	0.038 (4)	0.291 (11)	12g	
Sample C7029							
Octahedral sheet							
Mg	0.3333	0.6667	0.4999 (2)	0.0100 (3)	0.3333 *	4d	
Al	0	0	0.5000	0.0124 (4)	0.1667 *	2b	$Mg_4Al_2(OH)_{12}$
O1	0.3228 (4)	0.3227 (5)	0.5655 (1)	0.0176 (4)	1 *	12g	
H1	0.341 (10)	0.314 (10)	0.625 (2)	0.034 (11)	1 *	12g	

Table 2. *Cont.*

Atom	x	y	Z	U_{eq}	s.o.f.	W.P.	Assigned Site Populations
Interlayer gallery							
C1	0.3333	0.6667	0.748 (6)	0.025 (9)	0.033 *	4d	$(CO_3)_{1.0}(H_2O)_{2.9}$ **
C2	0.363 (4)	0	0.7500	0.021 (6)	0.050 *	6f	
O2	0.291 (3)	0.210 (3)	0.7497 (12)	0.038 (3)	0.272 (11)	12g	
O3	0.360 (3)	0.440 (3)	0.7500 (14)	0.042 (3)	0.279 (11)	12g	

* fixed during refinement; ** electron per formula unit (*epfu*) for O2 and O3 sites is recalculated as $(H_2O)^0$. W.P.—Wyckoff position.

The Mg and Al sites are ordered according to a $\sqrt{3} \times \sqrt{3}$ superstructure, and each of the metal sites is coordinated by six protonated oxygen atoms. The average <Mg–O> and <Al–O> bond distances are in the ranges 2.022–2.053 Å and 1.974–1.978 Å, respectively (Table 3). The other four sites, C1, C2, O2 and O3, are at the interlayer level and correspond to the low-occupied sites of statistically disordered $(CO_3)^{2-}$ groups and $(H_2O)^0$ molecules. All interlayers are identical and consist of both $(CO_3)^{2-}$ groups and $(H_2O)^0$ molecules in one layer.

Table 3. Selected bond distances (Å) for quintinite samples 91002 and C7029.

Atom	Atom	Bond Distance		Atom	Atom	Bond Distance	
		91002	C7029			91002	C7029
Mg	O1	2.027 (3)	2.053 (3)	C1	O3	1.275 (10)	1.277 (11)
Mg	O1 [1]	2.022 (2)	2.051 (2)	C2	O2	1.317 (16)	1.348 (16)
Al	O1	1.974 (2)	1.978 (2)	C2	O3 [1]	1.304 (14)	1.308 (14)

[1] Oxygen atoms, equivalent to O1 and O3, respectively, multiplied via symmetry elements.

The O1–H1 bond is nearly perpendicular to the plane of the octahedral sheet; the bond distance is 0.82/0.91 Å for samples 91002/C7029 (Table 4). The O1 atom acts as a donor (**D**), while the interlayer O2 and O3 atoms are acceptors (**A**) of hydrogen bonds. The **H** ··· **A** bond distance is almost two times longer than the **D**–**H** distance (Table 4).

Table 4. Hydrogen bonding scheme for quintinite samples 91002 and C7029.

Sample	D–H	*d* (D–H)	*d* (H ··· A)	<DHA	*d* (D ··· A)	A
91002	O1–H1	0.82 (4)	2.06(5)	168(4)	2.866(13)	O2
			2.06(5)	155(5)	2.823(13)	O2 [1]
			2.08(4)	157(5)	2.857(15)	O3
			2.01(5)	170(4)	2.826(15)	O3 [1]
C7029	O1–H1	0.91 (4)	1.96(4)	166(4)	2.850(19)	O2
			2.01(4)	154(5)	2.859(19)	O2 [1]
			2.00(4)	156(5)	2.86(2)	O3
			1.96(4)	170(4)	2.86(2)	O3 [1]

[1] Oxygen atoms, equivalent to O1 and O3, respectively, multiplied via symmetry elements.

3.2. Powder X-ray Diffraction

The main set of reflections of the powder X-ray diffraction pattern (Figure 4) correspond to the classic (for LDHs) 2*H* polytype (Table S1). Low-intensity superstructure reflection indicative of Mg and Al ordering according to a $\sqrt{3} \times \sqrt{3}$ superstructure is observed at d = 4.57 Å and indexed (*hkl*) as 010. Another characteristic feature of the quintinite powder X-ray diffraction pattern is the *d*-value of 7.56 Å, which agrees well with the previous crystal-chemical studies of quintinite [58].

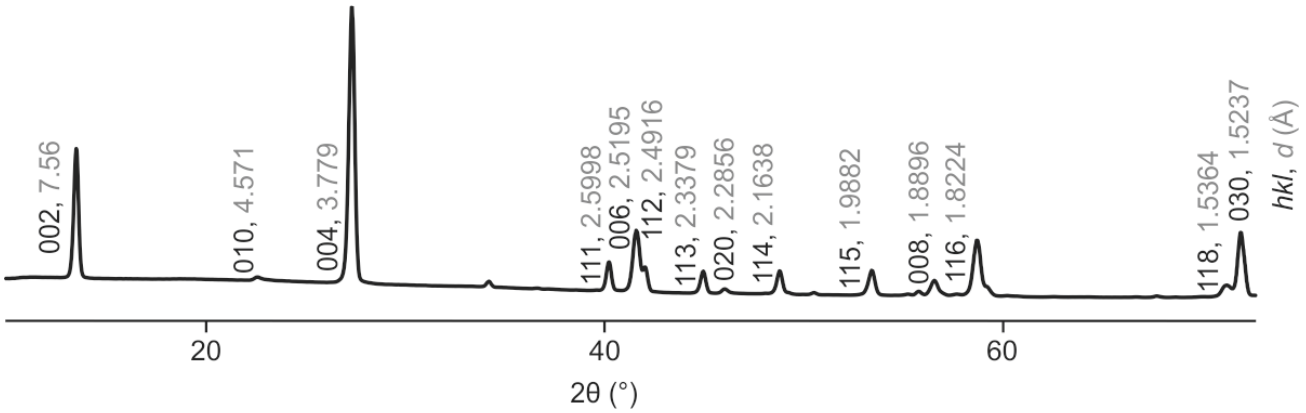

Figure 4. Indexed powder X-ray diffraction pattern of quintinite from Jacupiranga, sample 91002 {space group *P*-3*c*1; lattice parameters from powder X-ray diffraction data: a = 5.2783 (3) Å, c = 15.1171 (16) Å, V = 364.74 (6) Å^3}.

4. Discussion

In this work, using X-ray diffraction analysis, it is shown that quintinite from Jacupiranga is characterized by a hexagonal type of layer stacking, a superstructure based on Mg and Al ordering in a $\sqrt{3} \times \sqrt{3}$ pattern, and identical interlayers composed of disordered $(H_2O)^0$ molecules and $(CO_3)^{2-}$ groups at the same level in one gallery. This polytype is designated 2*T* according to the Ramsdell [59] notation. Topologically, quintinite-2*T* from Jacupiranga is identical to quintinite-2*T* from the Kovdor alkaline complex [42] and is the second confirmed finding of quintinite-2*T* in the world. It should be noted that, due to the high degree of disorder in the interlayer components, the positions of localized interlayer C and O atoms may differ from sample to sample. Despite that, the electron density distribution maps at the interlayer level are identical. The same is true of the space group selection, i.e., potential polytypes with structures refined in space groups *P*-3*c*1 or $P6_3/mcm$ with identical crystal-chemical features should not be taken as separate polytypes (see details in Section 2.2).

Previously, we assumed [42] that the structure obtained for quintinite from Jacupiranga [43] with stratified interlayers is not entirely correct from a crystal-chemical point of view, since, probably, the "carbonate" and "water" interlayers should have had different heights of the interlayer gallery, which was not observed. It should also be noted that such a division into two types of interlayers in the previous work was most likely because not all electron density peaks at the interlayer level were detected as their intensity could be very low, on the order of 1 $\bar{e}$. A similar problem is typical for earlier refinements of many LDH minerals and is a consequence of the (apparently) insufficient accuracy of equipment at that time. Although we had no opportunity to examine the same quintinite crystal as earlier researchers [43], we suggest that quintinite does not form structures with stratified interlayers. We also suggest that quintinite is characterized by four main polytypes (Figure 3), one of which is 2*T*, which is described in this work. We believe that this is a rather important assumption, since experimentally obtained crystal structures often become the basis for Rietveld refinements or computer simulation. Unfortunately, sometimes in the literature, it is possible to observe crystal structures that are unrealistic from a crystal-chemical point of view, in which, for example, H_2O molecules and carbonate groups are located in the same interlayer gallery at different levels.

The presence of M^{2+} and M^{3+} cation ordering within metal-hydroxide layers that form a $\sqrt{3} \times \sqrt{3}$ superstructure is manifested in the powder X-ray diffraction pattern by the presence of a superstructure reflection with $d \sim 4.57$ Å (indexed as 010 in the case of 2*T* polytype). The same superstructure reflection was observed for chlormagaluminite [33]. The powder X-ray diffraction patterns for both minerals, quintinite and chlormagaluminite, were recorded using the Gandolfi technique, reducing the effect of the sample's preferred orientation along [001]. The presence of such a reflection is indicative of M^{2+} and M^{3+} cation

ordering that should further be combined with the layer stacking sequence. However, the absence of this reflection, especially considering its low intensity (i.e., difficulty of detection), should not be taken as an indication of the absence of cation ordering.

An indirect criterion for the topological identity of quintinites from different natural environments and places can be the value of the interlayer distance (*d*-value) of quintinite, which is ~7.56 Å (Table 5) (or slightly above if the Mg:Al ratio is higher than the ideal of 2:1 [58]). Quintinite findings from different localities around the globe and different genetic types are characterized by a steady d_{00n}-value, despite some differences in the physicochemical and thermodynamic conditions of the formation of the minerals (Table 5). Thus, we believe that the internal structure of the mineral indicates certain principles for the construction of metal-hydroxyl layers and interlayers, as well as their interactions within the crystal structure, which can be transferred to artificially obtained compounds. In particular, we emphasize that, under room conditions, we do not observe fundamental changes in the content of interlayer H_2O molecules and related structural transformations of quintinite.

Table 5. Quintinite worldwide findings and their unit-cell parameters.

Locality	**Kovdor, Russia**	**Mont Saint-Hilaire, Canada**	**Jacupiranga, Brazil**	**Bazhenovskoe Deposit, Russia**	**Ural Emerald Mines (Malyshevskoe), Russia**
Occurrence	Late-stage hydrothermal mineral			Metosomatic alteration	
d_{00n}-value (Å) [1]	7.53–7.59	7.57	7.58	7.56	7.51
a' (Å) [2]	3.03–3.065	3.05	3.05	3.050	3.021
Reference	[38,39,41,42]	[44]	[43]; this work	[46]	[45]
Locality	Western Moravia, Czech Republic	Ampere and Josephine seamounts of the North Atlantic	Caspian lowland, Russia	Strandel Kogel, Austria	
Occurrence	quartz-oligoclase pegmatites of spentinite rock	secondary in basalt voids	evaporites (saline deposits)	cavities of hauyn-nephelinite	
d_{00n}-value (Å)	7.60	7.56	7.56	7.57	
a' (Å)	3.05	?	3.042	3.035	
Reference	[60,61]	[62]	[63]	[49]	

[1] d_{00n}-value is the distance between two neighboring metal-hydroxide layers. [2] a' is the distance between two neighboring metal cations in one metal-hydroxide layer.

Finally, we would like to emphasize that, according to the available structural data for quintinites from different findings and differing in geological position, that is, different conditions of formation, the crystal structures are built in the same way: (i) the structure of the interlayers is the same, (ii) the structure of the octahedral sheet differs only in the recorded ordering of Mg and Al or absence of recorded ordering, i.e., "disordered" (although disorder may be apparent due to the incorporation of impurities) and (iii) different types of stacking of layers.

5. Conclusions

In this work, we refined the crystal structure of Jacupiranga quintinite and showed that, from a structural point of view, it is identical to the 2*T* polytype of Kovdor quintinite and consists of metal hydroxide layers $[Mg_4Al_2(OH)_{12}]^{2+}$ and $[(CO_3)(H_2O)_3]^{2-}$ interlayers. The Mg and Al ordering according to a $\sqrt{3} \times \sqrt{3}$ superstructure is detected via single-crystal X-ray diffraction and powder X-ray diffraction through the appearance of addi-

tional (to 2*H* pattern) low-intensity superstructure reflections, including the reflection with d_{010}~4.57Å in the powder pattern. Combining our data and data from the literature, as well as information on the d_{00n}-values of quintinites (d_{00n}~7.56 Å) of various genetic types and localities, we conclude that the structure of quintinite obeys certain crystal chemical principles and is sustained in the light of layer–interlayer interactions and construction of octahedral sheets and interlayers. We consider it highly probable that quintinite polytypes already known from the Kovdor alkaline complex can be found in other localities, as shown in the example of quintinite from the Jacupiranga alkaline complex. In addition, we also hope that a more detailed history of the description of quintinite from Jacupiranga will lead to a correct definition of this mineral, which will help streamline the literature data on the description of hydrotalcite and quintinite.

Supplementary Materials: The following supporting information can be downloaded at: https://www.mdpi.com/article/10.3390/cryst13050839/s1, Table S1: Powder X-ray diffraction data for quintinite sample 91002; Table S2: Anisotropic displacement parameters (Å^2) for quintinite samples 91002 and C7029.

Author Contributions: Conceptualization, E.S.Z. and S.V.K.; methodology, E.S.Z., A.A.Z. and S.V.K.; software, E.S.Z., R.M.S., A.A.Z. and S.V.K.; validation, E.S.Z., R.M.S., A.A.Z. and S.V.K.; formal analysis, E.S.Z. and R.M.S.; investigation, E.S.Z., R.M.S., A.A.Z. and S.V.K.; resources, S.V.K.; data curation, E.S.Z. and A.A.Z.; writing—original draft preparation, E.S.Z., R.M.S. and S.V.K.; writing—review and editing, E.S.Z., R.M.S., A.A.Z. and S.V.K.; visualization, E.S.Z.; project administration, E.S.Z.; funding acquisition, E.S.Z. All authors have read and agreed to the published version of the manuscript.

Funding: This research was funded by Russian Science Foundation, grant number 22-77-10036.

Data Availability Statement: Crystallographic information files (cif) have been deposited via the joint Cambridge Crystal Data Centre CCDC/FIZ Karlsruhe deposition service; the deposition numbers are CSD 2260275 and 2260276 for samples 91002 and C7029, respectively.

Acknowledgments: The technical support of St. Petersburg State University Resource Centers "XRD" is gratefully acknowledged. We thank the Fersman Mineralogical Museum (Dmitry Belakovsky) and the Smithsonian National Museum of Natural History (Jeffrey Post) for providing the samples for research.

Conflicts of Interest: The authors declare no conflict of interest.

References

1. Mills, S.J.; Christy, A.G.; Génin, J.M.; Kameda, T.; Colombo, F. Nomenclature of the hydrotalcite supergroup: Natural layered double hydroxides. *Mineral. Mag.* **2012**, *76*, 1289–1336. [CrossRef]
2. Rives, V. *Layered Double Hydroxides: Present and Future*; Nova Science Publishers: New York, NY, USA, 2001; pp. 1–439.
3. Duan, X.; Evans, D.G. *Layered Double Hydroxides*; Springer: Berlin, Germany, 2006; pp. 1–87. [CrossRef]
4. Aminoff, G.; Broome, B. Contributions to the mineralogy of Långban. III. Contributions to the knowledge of the mineral pyroaurite. *K. Sven. Vetensk. Akad. Handl.* **1931**, *9*, 23–48.
5. Bukhtiyarova, M.V. A review on effect of synthesis conditions on the formation of layered double hydroxides. *J. Solid State Chem.* **2019**, *269*, 494–506. [CrossRef]
6. Yu, J.; Wang, Q.; O'Hare, D.; Sun, L. Preparation of two dimensional layered double hydroxide nanosheets and their applications. *Chem. Soc. Rev.* **2017**, *46*, 5950–5974. [CrossRef] [PubMed]
7. Kameliya, J.; Verma, A.; Dutta, P.; Arora, C.; Vyas, S.; Varma, R.S. Layered Double Hydroxide Materials: A Review on Their Preparation, Characterization, and Applications. *Inorganics* **2023**, *11*, 121. [CrossRef]
8. Rius, J.; Allmann, R. The superstructure of the double layer mineral wermlandite $[Mg_7(Al_{0.57},Fe^{3+}{}_{0.43})_2(OH)_{18}]^{2+}[(Ca_{0.6},Mg_{0.4})(SO_4)_2(H_2O)_{12}]^{2-}$. *Z. fur Krist.* **1984**, *168*, 133–144. [CrossRef]
9. Zhitova, E.S.; Chukanov, N.V.; Jonsson, E.; Pekov, I.V.; Belakovskiy, D.I.; Vigasina, M.F.; Zubkova, N.V.; Van, K.V.; Britvin, S.N. Erssonite, $CaMg_7Fe^{3+}{}_2(OH)_{18}(SO_4)_2{\cdot}12H_2O$, a new hydrotalcite-supergroup mineral from Långban, Sweden. *Mineral. Mag.* **2021**, *85*, 817–826. [CrossRef]
10. Huminicki, D.M.C.; Hawthorne, F.C. The crystal structure of nikischerite, $NaFe_6{}^{2+}Al_3(SO_4)_2(OH)_{18}(H_2O)_{12}$, a mineral of the shigaite group. *Can. Mineral.* **2003**, *41*, 79–82. [CrossRef]

11. Cooper, M.A.; Hawthorne, F.C. The crystal structure of shigaite, $[AlMn_2^{2+}(OH)_6]_3(SO_4)_2Na(H_2O)_6(H_2O)_6$, a hydrotalcite group mineral. *Can. Mineral.* **1996**, *34*, 91–97.
12. Sotiles, A.R.; Gomez, N.A.G.; Santos, M.P.; Grassi, M.T.; Wypych, F. Synthesis, characterization, thermal behavior and exchange reactions of new phases of layered double hydroxides with the chemical composition $[M^{+2}{}_6Al_3(OH)_{18}(SO_4)_2]$. $(A(H_2O)_6).6H2O$ (M^{+2} = Co, Ni; A = Li^+, Na^+, K^+). *Appl. Clay Sci.* **2019**, *181*, 105217. [CrossRef]
13. Sotiles, A.R.; Baika, L.M.; Grassi, M.T.; Wypych, F. Cation exchange reactions in layered double hydroxides intercalated with sulfate and alkali cations $(A(H_2O)_6)[M^{+2}{}_6Al_3(OH)_{18}(SO_4)_2].6H_2O$ (M^{+2} = Mn, Mg, Zn, A^+ = Li, Na, K). *J. Am. Chem. Soc.* **2019**, *141*, 531–540. [CrossRef] [PubMed]
14. Sotiles, A.R.; Wypych, F. Synthesis and topotactic exchange reactions of new layered double hydroxides intercalated with ammonium/sulfate. *Solid State Sci.* **2020**, *106*, 106304. [CrossRef]
15. Serna, C.J.; Rendon, J.L.; Iglesias, J.E. Crystal-chemical study of layered $[Al_2Li(OH)_6]^+X^-{\cdot}nH_2O$. *Clay Clay Miner.* **1982**, *30*, 180–184. [CrossRef]
16. Sissoko, I.; Iyagba, E.T.; Sahai, I.; Biloen, P. Anion intercalation and exchange in $Al(OH)_3$– derived compounds. *J. Solid State Chem.* **1985**, *60*, 283–288. [CrossRef]
17. Karcz, R.; Napruszewska, B.D.; Walczyk, A.; Kryściak-Czerwenka, J.; Duraczyńska, D.; Płaziński, W.; Serwicka, E.M. Comparative Physicochemical and Catalytic Study of Nanocrystalline Mg-Al Hydrotalcites Precipitated with Inorganic and Organic Bases. *Nanomaterials* **2022**, *12*, 2775. [CrossRef] [PubMed]
18. Karcz, R.; Napruszewska, B.D.; Michalik, A.; Kryściak-Czerwenka, J.; Duraczyńska, D.; Serwicka, E.M. Fine Crystalline Mg-Al Hydrotalcites as Catalysts for Baeyer-Villiger Oxidation of Cyclohexanone with H_2O_2. *Catalysts* **2021**, *11*, 1493. [CrossRef]
19. Yin, X.; Hua, Y.; Gao, Z. Two-Dimensional Materials for High-Performance Oxygen Evolution Reaction: Fundamentals, Recent Progress, and Improving Strategies. *Renewables* **2023**, *1*, 190–226. [CrossRef]
20. Leão, A.D.; Oliveira, V.V.; Marinho, F.A.; Wanderley, A.G.; Aguiar, J.S.; Silva, T.G.; Soare, M.F.R.; Soares-Sobrinho, J.L. Hybrid systems of glibenclamide and layered double hydroxides for solubility enhancement for the treatment of diabetes mellitus II. *Appl. Clay Sci.* **2019**, *181*, 105218. [CrossRef]
21. Francius, G.; André, E.; Soulé, S.; Merlin, C.; Carteret, C. Layered Double Hydroxides (LDH) as nanocarriers for antimicrobial chemotherapy: From formulation to targeted applications. *Mater. Chem. Phys.* **2023**, *293*, 126965. [CrossRef]
22. Kim, J.; Kim, T.H.; Lee, J.H.; Park, Y.A.; Kang, Y.J.; Ji, H.G. Porous nanocomposite of layered double hydroxide nanosheet and chitosan biopolymer for cosmetic carrier application. *Appl. Clay Sci.* **2021**, *205*, 106067. [CrossRef]
23. Zaghloul, A.; Benhiti, R.; Ichou, A.A.; Carja, G.; Soudani, A.; Zerbet, M.; Sinan, F.; Chiban, M. Characterization and application of MgAl layered double hydroxide for methyl orange removal from aqueous solution. *Mater. Today* **2021**, *37*, 3793–3797. [CrossRef]
24. Grégoire, B.; Bantignies, J.L.; Le-Parc, R.; Prélot, B.; Zajac, J.; Layrac, G.; Tichit, D.; Martin-Gassin, G. Multiscale mechanistic study of the adsorption of methyl orange on the external surface of layered double hydroxide. *J. Phys. Chem. C* **2019**, *123*, 22212–22220. [CrossRef]
25. Zhao, D.; Sheng, G.; Hu, J.; Chen, C.; Wang, X. The adsorption of Pb (II) on Mg2Al layered double hydroxide. *Chem. Eng. J.* **2011**, *171*, 167–174. [CrossRef]
26. Yang, X.; Kameda, T.; Saito, Y.; Kumagai, S.; Yoshioka, T. Investigation of the mechanism of Cu (II) removal using Mg-Al layered double hydroxide intercalated with carbonate: Equilibrium and pH studies and solid-state analyses. *Inorg. Chem. Commun.* **2021**, *132*, 108839. [CrossRef]
27. Nestroinaia, O.V.; Ryltsova, I.G.; Yaprintsev, M.N.; Nakisko, E.Y.; Seliverstov, E.S.; Lebedeva, O.E. Sorption of Congo Red anionic dye on natural hydrotalcite and stichtite: Kinetics and equilibrium. *Clay Miner.* **2022**, *57*, 105–113. [CrossRef]
28. Guo, J.Y.; Zhang, W.; Zhao, X.J.; Jie, Y.; Song, H.T.; Xu, X.Y.; Lu, H.; Yan, H. Theoretical Study on the Mechanism of Removing Harmful Anions from Soil via Mg2al Layered Double Hydroxide as Stabilizer. *SSRN* **2022**. [CrossRef]
29. Ke, X.; Bernal, S.A.; Provis, J.L. Uptake of chloride and carbonate by Mg-Al and Ca-Al layered double hydroxides in simulated pore solutions of alkali-activated slag cement. *Cem. Concr. Res.* **2017**, *100*, 1–13. [CrossRef]
30. Sakai, M.; Imagawa, H.; Baba, N. Layered-double-hydroxide-based Ni catalyst for CO_2 capture and methanation. *Appl. Catal. A-Gen.* **2022**, *647*, 118904. [CrossRef]
31. Zhitova, E.S.; Sheveleva, R.M.; Kasatkin, A.V.; Zolotarev, A.A.; Bocharov, V.N.; Kupchinenko, A.N.; Belakovsky, D.I. Crystal structure of hydrotalcite group mineral—Desautelsite, $Mg_6Mn^{III}{}_2(OH)_{16}(CO_3){\cdot}4H_2O$, and relationship between cation size and in-plane unit cell parameter. *Symmetry* **2023**, *15*, 1029. [CrossRef]
32. Karpenko, V.Y.; Zhitova, E.S.; Pautov, L.A.; Agakhanov, A.A.; Siidra, O.I.; Krzhizhanovskaya, M.G.; Rassulov, V.A.; Bocharov, V.N. Akopovaite, $Li_2Al_4(OH)_{12}(CO_3)(H_2O)_3$, a new Li-member of the hydrotalcite supergroup from Turkestan Range, Kyrgyzstan. *Mineral. Mag.* **2020**, *84*, 301–311. [CrossRef]
33. Zhitova, E.S.; Krivovichev, S.V.; Pekov, I.V.; Yapaskurt, V.O. Crystal chemistry of chlormagaluminite, $Mg_4Al_2(OH)_{12}Cl_2(H_2O)_2$, a natural layered double hydroxide. *Minerals* **2019**, *9*, 221. [CrossRef]
34. Zhitova, E.S.; Pekov, I.V.; Chaikovskiy, I.I.; Chirkova, E.P.; Yapaskurt, V.O.; Bychkova, Y.V.; Belakovsky, D.I.; Chukanov, N.V.; Zubkova, N.V.; Krivovichev, S.V.; et al. Dritsite, $Li_2Al_4(OH)_{12}Cl_2{\cdot}3H_2O$, a new gibbsite-based hydrotalcite supergroup mineral. *Minerals* **2019**, *9*, 492. [CrossRef]

35. Britto, S.; Thomas, G.S.; Kamath, P.V.; Kannan, S. Polymorphism and structural disorder in the carbonate containing layered double hydroxide of Li with Al. *J. Phys. Chem.* **2008**, *112*, 9510–9515. [CrossRef]
36. Britto, S.; Kamath, P.V. Structure of Bayerite-Based Lithium–Aluminum Layered Double Hydroxides (LDHs): Observation of Monoclinic Symmetry. *Inorg. Chem.* **2009**, *48*, 11646–11654. [CrossRef]
37. Britto, S.; Kamath, P.V. Polytypism in the lithium–aluminum layered double hydroxides: The $[LiAl_2(OH)_6]^+$ layer as a structural synthon. *Inorg. Chem.* **2011**, *50*, 5619–5627. [CrossRef] [PubMed]
38. Krivovichev, S.V.; Yakovenchuk, V.N.; Zhitova, E.S.; Zolotarev, A.A.; Pakhomovsky, Y.A.; Ivanyuk, G.Y. Crystal chemistry of natural layered double hydroxides. I. Quintinite-2*H*-3 c from the Kovdor alkaline massif, Kola peninsula, Russia. *Mineral. Mag.* **2010**, *74*, 821–832. [CrossRef]
39. Krivovichev, S.V.; Yakovenchuk, V.N.; Zhitova, E.S.; Zolotarev, A.A.; Pakhomovsky, Y.A.; Ivanyuk, G.Y. Crystal chemistry of natural layered double hydroxides. 2. Quintinite-1*M*: First evidence of a monoclinic polytype in M^{2+}-M^{3+} layered double hydroxides. *Mineral. Mag.* **2010**, *74*, 833–840. [CrossRef]
40. Krivovichev, S.V.; Yakovenchuk, V.N.; Zhitova, E.S. Natural double layered hydroxides: Structure, chemistry, and information storage capacity. In *Minerals as Advanced Materials II*; Krivovichev, S.V., Ed.; Springer: Berlin/Heidelberg, Germany, 2012; pp. 87–102. [CrossRef]
41. Zhitova, E.S.; Yakovenchuk, V.N.; Krivovichev, S.V.; Zolotarev, A.A.; Pakhomovsky, Y.A.; Ivanyuk, G.Y. Crystal chemistry of natural layered double hydroxides. 3. The crystal structure of Mg, Al-disordered quintinite-2*H*. *Mineral. Mag.* **2010**, *74*, 841–848. [CrossRef]
42. Zhitova, E.S.; Krivovichev, S.V.; Yakovenchuk, V.N.; Ivanyuk, G.Y.; Pakhomovsky, Y.A.; Mikhailova, J.A. Crystal chemistry of natural layered double hydroxides: 4. Crystal structures and evolution of structural complexity of quintinite polytypes from the Kovdor alkaline-ultrabasic massif, Kola peninsula, Russia. *Mineral. Mag.* **2018**, *82*, 329–346. [CrossRef]
43. Arakcheeva, A.V.; Pushcharovskii, D.Y.; Rastsvetaeva, R.K.; Atencio, D.; Lubman, G.U. Crystal structure and comparative crystal chemistry of $Al_2Mg_4(OH)_{12}(CO_3)\cdot 3H_2O$, a new mineral from the hydrotalcite-manasseite group. *Crystallogr. Rep.* **1996**, *41*, 972–981.
44. Chao, G.Y.; Gault, R.A. Quintinite-2*H*, quintinite-3*T*, charmarite-2*H*, charmarite-3*T* and caresite-3*T*, a new group of carbonate minerals related to the hydrotalcite-manasseite group. *Can. Mineral.* **1997**, *35*, 1541–1549.
45. Zhitova, E.S.; Popov, M.P.; Krivovichev, S.V.; Zaitsev, A.N.; Vlasenko, N.S. Quintinite-1M from the Mariinsky Deposit, Ural Emerald Mines, Central Urals, Russia. *Geol. Ore Depos.* **2018**, *59*, 745–751. [CrossRef]
46. Krivovichev, S.V.; Antonov, A.A.; Zhitova, E.S.; Zolotarev, A.A.; Krivovichev, V.G.; Yakovenchuk, V.N. Quintinite-1M from Bazhenovskoe deposit (Middle Ural, Russia): Crystal structure and properties. *Vestnik Saint Petersburg Univ. Earth Sci.* **2012**, *7*, 3–9. (In Russian)
47. Piilonen, P.; Poirier, G.; Rowe, R.; Mitchell, R.; Robak, C. Mount Mather Creek, British Columbia—A new sodalite-bearing carbohydrothermal breccia deposit including a new Canadian occurrence for the rare minerals edingtonite and quintinite. *Mineral. Mag.* **2022**, *86*, 282–306. [CrossRef]
48. Menezes, L.A.D.; Martins, J.M. The Jacupiranga mine Sao-Paulo, Brazil. *Mineral. Rec.* **1984**, *15*, 261–270.
49. Alker, A.; Golob, P.; Postl, W.; Waltinger, H. Hydrotalkit, Nordstrandit und Motukoreait vom Stradner Kogel, südlich Gleichenberg, Steiermark. Mitt.-Bl. Abt. Mineral. *Landesmuseum Joanneum* **1981**, *49*, 1–13.
50. Mills, S.J.; Christy, A.G.; Schmitt, R. The creation of neotypes for hydrotalcite. *Mineral. Mag.* **2016**, *80*, 1023–1029. [CrossRef]
51. Raade, G. Hydrotalcite and quintinite from Dypingdal, snarum, Buskerud, Norway. *Norsk Bergverksmuseum Skrifter* **2013**, *50*, 55–57.
52. Oliveira, S.B.D.; Sant'Agostino, L.M. Lithogeochemistry and 3D geological modeling of the apatite-bearing Mesquita Sampaio beforsite, Jacupiranga alkaline complex, Brazil. *Brazil. J. Geol.* **2020**, *50*, e20190071. [CrossRef]
53. *CrysAlisPro Software System, Version 1.171.38.46*; Rigaku Oxford Diffraction: Oxford, UK, 2015.
54. Sheldrick, G.M. Crystal structure refinement with SHELXL. *Acta Crystallogr. A* **2015**, *71*, 3–8. [CrossRef]
55. Dolomanov, O.V.; Bourhis, L.J.; Gildea, R.J.; Howard, J.A.; Puschmann, H. OLEX2: A complete structure solution, refinement and analysis program. *J. Appl. Crystallogr.* **2009**, *42*, 339–341. [CrossRef]
56. Britvin, S.N.; Dolivo-Dobrovolsky, D.V.; Krzhizhanovskaya, M.G. Software for processing of X-ray powder diffraction data obtained from the curved image plate detector of Rigaku RAXIS Rapid II diffractometer. *Zapiski RMO* **2017**, *146*, 104–107. (In Russian)
57. *TOPAS V4.2: General Profile and Structure Analysis Software for Powder Diffraction Data*; Bruker-AXS: Karlsruhe, Germany, 2009.
58. Zhitova, E.S.; Krivovichev, S.V.; Pekov, I.V.; Yakovenchuk, V.N.; Pakhomovsky, Y.A. Correlation between the d-value and the M^{2+}:M^{3+} cation ratio in Mg–Al–CO_3 layered double hydroxides. *Appl. Clay Sci.* **2016**, *130*, 2–11. [CrossRef]
59. Guinier, A.; Bokij, G.B.; Boll-Dornberger, K.; Cowley, J.M.; Ďurovič, S.; Jagodzinski, H.; Krishna, P.; de Woff, P.M.; Zvyagin, B.B.; Cox, D.E.; et al. Nomenclature of polytype structures. Report of the International Union of Crystallography Ad hoc Committee on the nomenclature of disordered, modulated and polytype structures. *Acta Crystallogr. A* **1984**, *40*, 399–404. [CrossRef]
60. Černý, P. Hydrotalcite z Vézná na zapadni Morave. *Acta Musei Moraviae* **1963**, *XLVII*, 23–30.
61. Allmann, R.; Jespen, H.P. Die struktur des hydrotalkits. *Neues Jahrbuch Für Mineralogie Monatshefte* **1969**, *1969*, 544–551.

62. Lisitsina, V.A.; Drits, V.A.; Sokolova, T.N. New complex of secondary minerals-products of low temperature transformations of rocks, covering basalts of Atlantic Ocean underwater mountains. *Lithol. Miner. Resour.* **1985**, *6*, 20–39.
63. Drits, V.A.; Sokolova, T.N.; Sokolova, G.V.; Cherkashin, V.I. New members of the hydrotalcite—Manasseite group. *Clays Clay Miner.* **1987**, *35*, 401–417. [CrossRef]